# Disentangling the power transfer process by non-contact optical measurement in nickel-zinc ferrite/piezoelectric magnetoelectric gyrators

Jitao Zhang[1†], Hewei Zhao[1], Qingfang Zhang[1], D. A. Filippov[2], Jie Wu[1], Jiagui Tao[3], Liying Jiang[1†], Lingzhi Cao[1] and Gopalan Srinivasan[4]

[1]College of Electrical and Information Engineering, Zhengzhou University of Light Industry, Zhengzhou 450002, China

[2]Institute of Electronic and Information Systems, Novgorod State University, Veliky Novgorod 173003, Russia

[3]State Grid of Jiangsu Electric Power Co., Ltd. Nanjing 210024, China

[4]Physics Department, Oakland University, Rochester, Michigan 48309, USA

To precisely position the main energy dissipation sources in ferrite/piezoelectric ME-coil gyrators, the dynamic magneto-mechanical-electric conversion process was disentangled quantitatively by employing a non-contact optical measurement methodology. For the sample fabrication, successful crystallization as well as desired magnetic properties for sintered spinel ferrites was confirmed by XRD and SQUIDs measurements. Trapped magnetic energies in ferrites will convert into kinetic energies accompanying indispensable dissipations in this dynamic process, and the converted kinetic energies can be measured quantitatively in the form of vibrating velocity by focused laser beam. As a result, only ~71% of mechanical energies can be transferred successfully to next layer due to the influence of adhesive in tri-layer sample while the value is 57% for bi-layer one. Finally, comparative studies of low-frequency/resonance ME interactions and power conversion efficiency in tri-layer and bi-layer samples were measured, and an eventual maximum PE of 80.3% under optimum load of 3.5kΩ was achieved. We infer from the results that the mechanical loss between layers is still a bottleneck to block the efficient energy transfer. These findings provide a deep analysis to reveal the dynamic energy transfer in ME-coil gyrators as well as a flexible pathway for ME gyrators design.

## 1. Introduction

As the missing fifth basic electric network element, gyrator featured passive, linear, lossless and nonreciprocal merits was conjectured by Tellegen in 1948, which permits the direct conversion between current and voltage or vice versa accompanying capacitance/inductance inverted between its two ports.[1] In practical, gyrators can be employed to build an inductor with capacitors, and the major benefit is that an equivalent inductance can be implemented and substituted by a much smaller physically sized capacitator to be more easily integrated. In light of versatile pathways suggested by Tellegen to build a practical gyrator, the subsequent studies with more attempts to realize the gyrators were implemented with an operational amplifier and some additional passive components.[2] Eventually, the gyrators with some end cutting-edge applications can be deployed in impedance matching, energy transmission or electric isolation *etc*.[3-6]

With the upsurge of the multiferroic ME composites research appeared in the early 2000s,

† Corresponding author: Tel. /Fax: +86 371 86601601.
E-mail *address:* zhangjitao@zzuli.edu.cn (J. T. Zhang) and jiangliying@zzuli.edu.cn (L. Y. Jiang)

multiferroic materials with stronger ME couplings at room temperature did not exist before 2001 and thus passive gyrators were not successfully developed.[7-9] Therefore, the emergence of magnetoelectric (ME) laminates and devices offer an alternative passive approach and enhanced flexibility for the gyrator realizations due to their underlying physics of induced polarization in an applied magnetic field or vice versa, thereby the ME composite with solenoid wound around is likely candidate for ME gyration devices.[10-12] Initially, the definition and structural scheme for 4-wire 2-port ME gyrators were explicated by Zhai *et al*. in 2006, and evidence for strong gyration effects was observed.[13] Meanwhile, for the energy conversion ME devices, much effort has been devoted to improving the ME couplings for energy scavenging, and the maximum output power density under optimum resistance load connected is reckoned as an indispensable parameter to examine the performance of ME harvesters.[14-16] Correspondingly, gyrator was usually integrated in non-reciprocal phase shifters, frequency-conversion isolators, and high-linearity/high-frequency/ultra-broadband circulators with energy conversion involved.[17-19] As such, power conversion efficiency (PE) is employed to evaluate the performance of ME gyrators borrowing from the characterizations of ME harvester. Although there have been considerable research activities on bulk and layered ME composite-coil gyrators, recent advances in ME gyrators revived by DAPAR MATRIX program are focused on PE improvement.[20-23] Methodologies for PE enhancement can be roughly classified into three categories: structural optimization, materials selection and size reduction.[24-26] Main contribution of structural optimization in ME gyrators was presented by Leung *et al.* in 2017, two types ME-coil gyrators of magnetostrictive/piezoelectric/magnetostrictive (M-P-M) laminate and piezoelectric/magnetostrictive/piezoelectric (P-M-P) laminate were designed and characterized, results showed that the P-M-P one exhibits a higher PE of ~85% under EMR driving and optimum bias field of 40Oe.[27] Regarding the materials selection, in 2019 Zhang *et al.* reported an efficient ME gyrator consisting of nickel-iron-based constant elasticity alloy with high quality factor (~1082) and piezoelectric ceramics, yielding a maximum PE as high as 88.5% under extremely low input power density of 3.31μW/cm$^3$.[28] Very recently in 2020, Zhuang *et al.* reported an efficient, compact ME gyrator consisting of Mn-doped $Pb(Mg_{1/3}Nb_{2/3})O_3$-$PbTiO_3$ (PMN-PT) single crystal and Metglas foils, achievable PE as high as ~92% was obtained with dramatically decreased size as compared with the similar one made of "hard" PZT ceramics.[29] To data, the highest PE of ~95% has been found in Metglas/PMN-PZT ME gyrators, whereby the magnetic and electric energy were efficiently coupled via strain across an interface between ferromagnetic and piezoelectric phases with approximately 5% of energy dissipation.[30] Although high PE value is a decisive parameter of ME gyrator, research on affecting factors of energy dissipation in magnetoelectric conversion process is necessary for further design of gyrators. Modeling efforts on theoretical analysis of expression between PE and the temperature increase within a heat-balanced system was implemented by Zhuang *et al*. recently in 2020, as a consequence the power efficiency variations can be monitored by this temperature rise.[31, 32] In fact, energy transfer undergoes a dynamic magneto-mechanical-electric process between two ports of the ME gyrators, and more or less indispensable energy dissipations occurred in the form of mechanical loss or heat in this process. However, the origins of the main energy dissipation from the whole dynamic energy conversion process is still unclear without works reported so far.

In this study, to disentangle the power transfer process, in-deep exploration for each stage of magneto-mechanical-electric conversion in ferrite/piezoelectric ME gyrator was implemented by

means of finite element method (FEM) and dynamic non-contact optical technology, anticipating the precise locating for the origins of energy dissipations in this process. High-quality Ni-Zn ferrite was synthesized by standard solid-state sintering techniques and its preferable crystallization and magnetic properties were confirmed by the X-ray diffraction (XRD) and SQUIDs characterizations. Meanwhile, low-frequency/resonance ME couplings and eventual PE were also measured to examine the methodology we employed to analyze the power transfer process. Further research progresses in this field for locating the energy dissipation in ME gyrators can lighten the future structure design and materials selection for device optimization.

## 2. Experimental details

Layered ME composite consisting of ferromagnetic ferrite and piezoelectric PZT-8 slab were synthesized using standard solid-state sintering techniques, and rare earth doped spinel ferrite of $Ni_{0.7}Zn_{0.3}Tb_{0.02}Fe_{1.98}O_4$ (NZTFO) was selected for following studies due to its high piezomagnetic coefficient (~40 ppm/Oe) and high quality factor (~300). Here terbium was doped in spinel nickel zinc ferrites with Zn substitution, and the iron ions were replaced with divalent ions that were chemically and structurally compatible with the spinel host lattice. More specifically, the divalent ions of $Tb^{3+}$ improve magnetocrystalline anisotropy and magnetostriction through magnetoelastic interactions with its ligand coordination.[33] Commercially available powders of NiO, ZnO, $Tb_4O_7$, and $Fe_2O_3$ were mixed, ball-milled and then calcinated at 1275°C with heating/cooling rate of 2ºC/min in a muffle furnace.[34] Calcinated ferrite blocks were cut into thin pieces with dimensions of 37×5×1 $mm^3$ and polished with 400-grit silicon-carbide paper to remove the surface scale or oxide. Hard piezoelectric ceramics of PZT-8 with high quality factor (~1000) and similar dimensions were purchased (Yuhai Electronic ceramics Co., Ltd, Zibo China), and their relative lower impedance (~800Ω@60kHz) is easily matched for the required resistance load. Layered ME laminate was then made with the ferromagnetic NZTFO platelet and piezoelectric PZT-8 slab bonded together using epoxy resin adhesive, and the solder terminals were introduced from each electrode surface of the PZT slab for the following measurement. Subsequently, the sample was cured at 100ºC under pressure load of 5MPa for 2h. Finally, the ME sample was centered in a small solenoid with 260-turn windings for necessary ready measurement. XRD was characterized by X-ray diffractometer (Bruker Model Advance D8) to make sure the faultless crystallization, and the magnetic properties were measured by physical property measurement system (PPMS-VSM, Quantum Design Model XL-7). For the magneto-mechanical conversion characterizations, laser Doppler vibrometer (Polytec Model OFV-5000/505) was employed for the vibrating velocity measurement, and the output signals in the form of voltage were captured by a lock-in amplifier (Zurich Instruments, Model MFLI 500kHz). Measurements of low-frequency/resonance ME couplings and PE were implemented by means of an automatic measurement system in lab, and more details can be found in our previously reported literatures.[35, 36]

## 3. Results and discussions

### *a. Materials characterizations*

For structural and magnetic characterization, the X-ray diffraction patterns of NZTFO bulk sample are depicted in Fig. 1(a). Significant diffraction peaks at (111), (220), (311), (222), (400), (422), (511) and (440) were observed clearly in coincidence with the emerging positions and relative intensities of standard XRD pattern in $Fe_3O_4$ (PDF#75-0449), and thus the successful

crystallization of spinel structure in calcinated ferrites was confirmed without any impurity phases. Figure 1(b) illustrates the perpendicular and parallel magnetic hysteresis loops for the NZTFO samples with dimensions of 3mm×2mm×1mm at room temperature, and the magnetization process exhibits an in-plane easy axis and an out-of-plane hard axis due to the size-induced demagnetization effects. Consequently, typical data on M *vs* H profile in terms of magnetocrystalline anisotropy with saturation magnetization $M_s$ increased from 60emu/g for in-plane to 69emu/g for out-of-plane, while a higher remnant magnetization $M_r$ of 3.12emu/g can be obtained for in-plane relative to 0.72emu/g for out-of-plane.

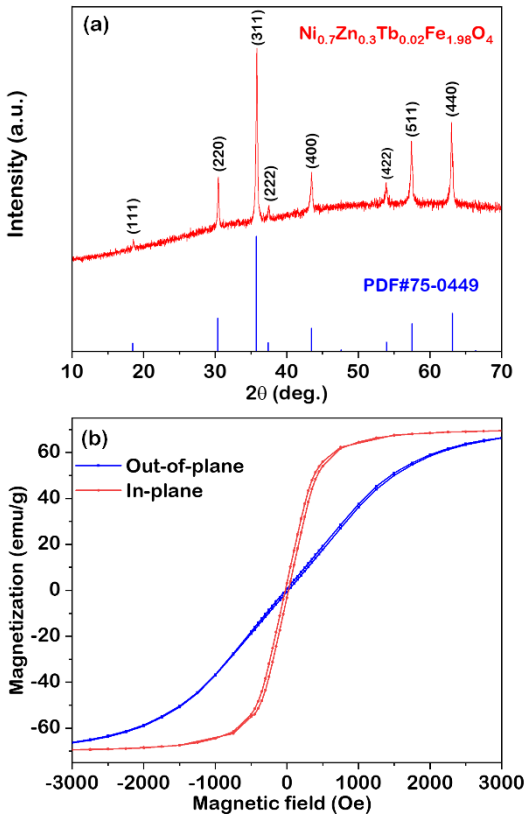


Fig.1(a) XRD pattern of $Ni_{0.7}Zn_{0.3}Tb_{0.02}Fe_{1.98}O_4$ polycrystalline bulk sample with standard one of $Fe_3O_4$ for comparison, (b)in-plane and out-of-plane magnetic hysteresis loops for $Ni_{0.7}Zn_{0.3}Tb_{0.02}Fe_{1.98}O_4$ platelet.

***b. Estimation of effective electric-magneto conversion***

According to the working principle of ME gyration effects, a dynamic electric-magneto-mechanical-electric conversion was involved in the whole energy transfer process, and necessary attempts to decompose this process were implemented to clarify each stage of energy transfer quantitatively. Firstly, electric-magneto conversion was characterized by FEM simulation to estimate the effective converted magnetic energy, and the spatial magnetic distribution as well as magnetic energy density can be obtained to calculate the absorbed magnetic energy into the ME sample. Specifically, simulation modeling for the device was built strictly in compliance with its actual size, parameters of radius $R$=5mm, turns $N$=260 and length $L$=40mm for a solenoid were assigned to the software for simulation, and the coordinate system was established as shown in Fig.2(a). $Z$ and $X$ axis designate the polarization and magnetization directions, respectively. The spinel ferrite was assigned the measured in-plane M *vs* H data to approximate its real properties,

and 25742 mesh points with boundary conditions were generated automatically for further calculations. The converged spatial magnetic flux lines inside the solenoid can be observed by taking advantage of the higher permeability of the ferrites. Magnetic flux density contrast image of *XY* plane was shown in Fig.2(b), and the magnetic flux density exhibits an ununiform contrast with the value decreased from center of the NZTFO layer to the edge due to generated magnetic field from finite length of the solenoid. In that case, downward opening parabola-like line scan traces along the axial center-line of the NZTFO layer were observed as illustrated in Fig. 2(c), *B* reaches its maximum of 0.34mT at the position of approximately $x$=18mm.

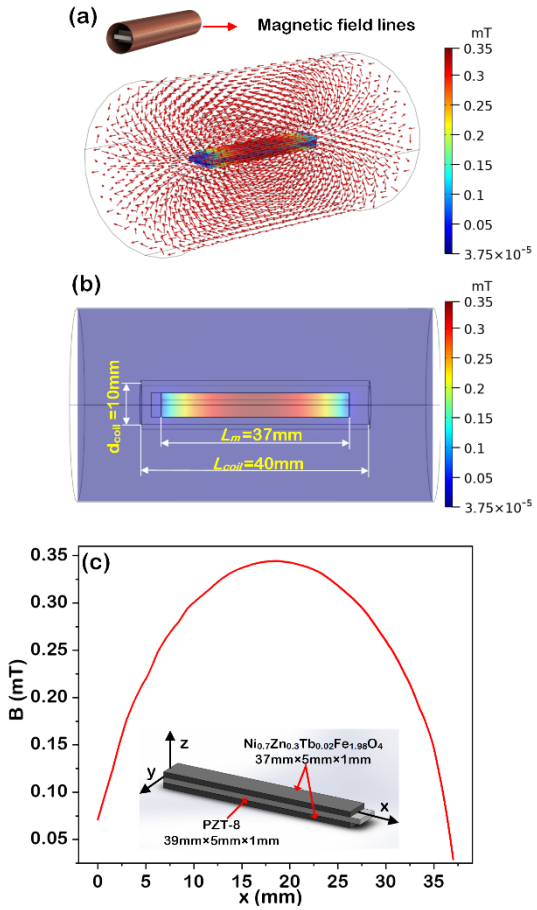


Fig. 2(a) Spatial magnetic field distributions for the presented device, and the arrows represent magnetic flux lines. The inset shows the schematic diagram of the ME gyrator. (b) Scanning contrast image showing the magnetic flux density of NZTFO layer in *XY* plane. (c) line scan traces of magnetic induction along the axial centerline of NZTFO platelet. The inset shows the established coordinate systems for ME gyrator modeling, *Z* and *X* axises designate the polarization and magnetization directions, respectively.

For the ME-coil gyrators, indispensable energy dissipations will occur in conversions from AC magnetic energy produced by AC current-carrying solenoid to trapped magnetic energy in ME sample, and the input total electric energies were roughly divided into two portions of the trapped in ferrite and the dissipated in air. To clarify quantitively the trapped magnetic amount in this process, the transient response of magnetic energy can be calculated by solving the equation of

$$W = \iiint (\frac{1}{T}\int_0^T H_m \cos(\omega t) dB_m \cos(\omega t - \delta)) dV \quad (1)$$

where $B_m cos(\omega t)$ and $H_m cos(\omega t-\delta)$ represent the dynamic magnetic induction strength and magnetic field strength to the excitation AC magnetic field with angular frequency of $\omega$, $\delta$ is the lagged angle of $B$, and d$V$ denotes differential of unit volume). Simulation results are shown in Fig. 3, magnetic energy density essentially exhibits a standard sinusoidal response and stabilizes at ~160ns with periods of 10ns, the following four stabilized periods in the range of 160-198ns were selected for further calculation. Consequently, higher density of 0.65mJ/m$^3$ trapped in NZTFO platelet was achieved relative to 0.03mJ/m$^3$ dissipated in spatial air domain, this generally means that the trapped energy (or magnetic flux lines) in ferrite exhibits approximately 22 times higher than that of air inside the solenoid if their volumes are assumed to be equal.

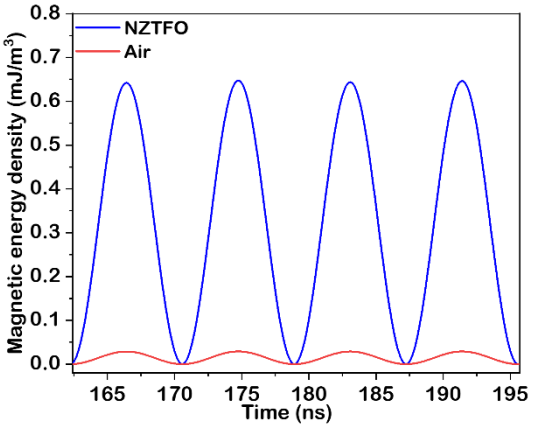


Fig.3 Transient responses of magnetic energy densities trapped in ferrites and dissipated in air.

### *c. Analysis of strain-mediated magneto-mechanical conversion*

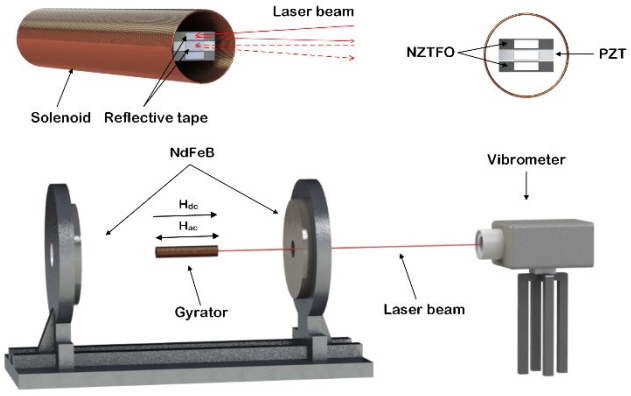


Fig.4 Schematic diagram of non-contact optical measurement system for vibrating velocity acquisition.

Input electric energy was partially transferred to magnetic energy via electromagnetic couplings of solenoid as mentioned above, and subsequently the trapped magnetic energy traveled dynamic magneto-mechanical conversion and enabled the ferrite layer to vibrate alternately along the driving frequency. In this process, dynamic magneto-mechanical conversion was mainly influenced by the physical properties of the magnetostrictive material and interlayer coupling via epoxy adhesive. To

clarify the energy dissipations quantitatively in this process, a non-contact optical methodology was introduced to capture the vibrating velocity then eventual kinetic energies layer by layer, and the corresponding measurement system was setup as illustrated in Fig. 4. A 633nm He-Ne laser beam emitted from the sensor head of doppler vibrometer was focused and then reflected at reflective tape attaching onto the end of ME laminate, thereby the velocity signal was decoded and then captured by VD-09 decoder and lock-in amplifier, respectively. A pair of toroidal NdFeB permanent magnets was employed to provide DC magnetic field to facilitate the laser beam passing through easily. In this case, vibrating velocity spectrum were obtained around the electromechanical resonance (EMR) frequency.

Experimental strategy for vibrating velocity measurement in the dynamic magneto-mechanical conversion process was listed in the following, and the single NZTFO platelet with/without attached PZT slab serving as mechanical load was characterized sequentially under constant input voltage of 200mV of the solenoid. Firstly, each layer for all samples were attached with reflective tape at their end surface, and a single NZTFO platelet with dimensions of $37\times5\times1mm^3$ was selected with the beam focused on the tape. Secondly, the focused beam was shifted to the PZT slab in bi-layer ME sample for measuring the transferred velocity. Thirdly, for comparative studies, similar characterizations were carried out for PZT slab in tri-layer ME sample. Results in Fig. 5 show the comparative diagram of velocity spectrum in the vicinity of EMR frequency for focused beam at single NZTFO platelet, PZT slab in bi-layer ME sample and PZT slab in tri-layer one, respectively. For the single NZTFO platelet, its velocity under free boundary vibrations reaches a maximum of 8.74mm/s at EMR frequency of 74.45kHz. To acquire the transferred velocity bi-layer ME laminate with PZT slab attached, resonance frequency of focused beam at PZT platelet decreased to 54.13kHz as well as the amplitude to 4.73mm/s due to the additional mechanical load. Compared with the bi-layer case, velocity spectrum shows a moderate rise in amplitude and EMR frequency in symmetric tri-layer sample, we infer from the results that this discrepancy is mainly attributed to the decreased average density/effective compliance coefficient and enhancement of actuating capability.[37, 38] Therefore, energy transfer occurred in the dynamic magneto-mechanical process from the trapped magnetic to mechanical vibrations, accompanying a velocity decrease with the PZT slab loaded.

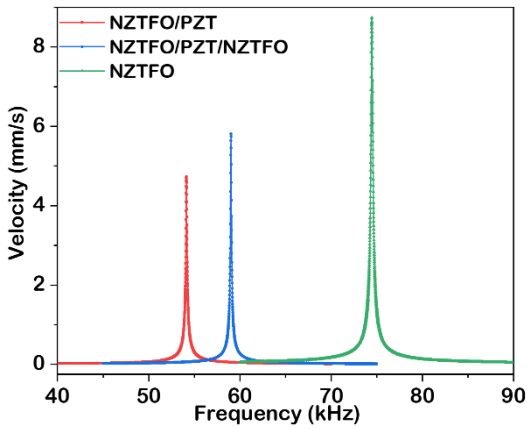


Fig.5 Velocity spectrum for the single NZTFO platelet, PZT slab in bi-layer ME sample and PZT slab in tri-layer ME sample in their vicinity of resonance frequencies, respectively.

More relevant explorations and discussions to follow, the laser beam was focused on NZTFO platelet first and then PZT slab in bi-layer ME sample, and the obtained velocity spectrum were shown in Fig. 6(a). We found that response curves show nearly coincident response with maximum velocity of 4.73mm/s at 54.13kHz for NZTFO layer and 4.87mm/s at 54.15kHz for PZT layer. Subsequently, as an additional mechanical load, PZT slab was laminated into ME sample, input and output strain-mediated energy between layers in the form of kinetic energy can be evaluated. Masses for single NZTFO and PZT platelets are 63.9mg and 154.8mg, respectively, and then the kinetic energy was calculated using the formula of $\int(1/2)mv^2dv$. As a result, comparative kinetic energy spectrum for single NZTFO and PZT slab in bi-layer laminate is illustrated in Fig.6(b), and maximum values of approximately 0.07nJ and 0.04nJ can be obtained at their resonance frequency. In other words, it means that nearly 43% kinetic energy was dissipated in this magneto-mechanical process for bi-layer sample. To further explore whether the different laminating scheme of ME composites can affect the kinetic energy dissipations between layers in dynamic magneto-mechanical process, similar measurements were performed in tri-layer symmetrical ME sample for tracking the energy dissipations. In this case, the actuating vibrating source is top/bottom two NZTFO layers, and the velocity spectrum for each layer of the tri-layer sample was shown in Fig. 6(c). Similarly, the three response curves for each layer remain essential coincident as expected, and the corresponding kinetic energy was calculated and plotted in Fig. 6(d). Maximum output kinetic energy form PZT layer reaches 0.1nJ while the input from two NZTFO platelets is 0.14nJ, much lower of approximately 29% kinetic energy was dissipated. Therefore, the mechanical energy dissipations in the form of kinetic energies were clarified quantitatively, and the mechanical loss between layers dominates the main dissipation sources.

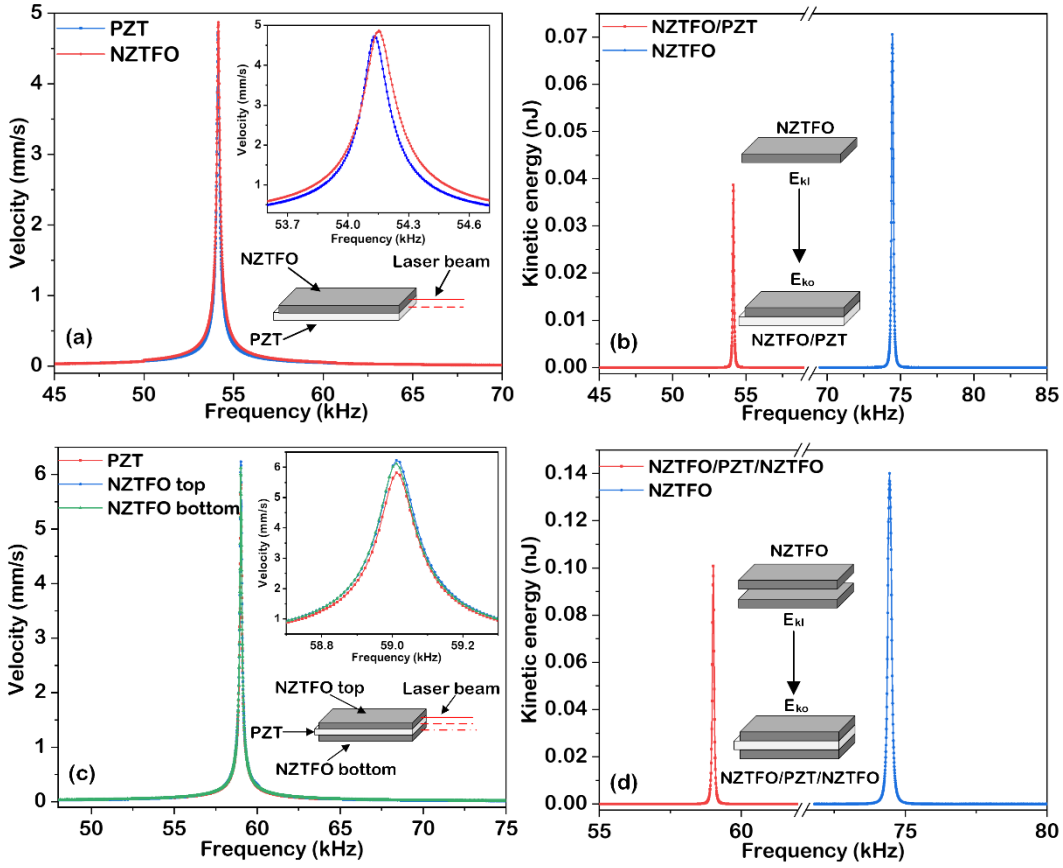


Fig.6(a) Velocity spectrum for each layer of PZT and NZTFO in bi-layer sample around resonance.

(b) Calculated kinetic energy spectrum for single NZTFO platelet and bi-layer sample, respective. (c)Velocity spectrum for each layer of PZT and NZTFO in tri-layer sample around resonance. (d) Calculated kinetic energy spectrum for two NZTFO platelet and tri-layer sample, respective.

***d. Measurement of magnetoelectric couplings and eventual conversion efficiency***

Finally, measurements of low-frequency/resonance ME couplings and eventual power conversion efficiencies were carried out, and tri-layer and bi-layer ME samples were selected for comparative studies of the ME conversion and eventual efficiency. Low-frequency ME interactions at off-resonance frequency of 10kHz with applied magnetic field sweeping for NZTFO/PZT/NZTFO and NZTFO/PZT samples were measured by an automatic measuring system, respectively, and the sequence for applied magnetic field was strictly followed by the standard magnetization measurement.[39] As illustrated in Fig. 7(a), the absolute value of magnetoelectric voltage coefficient |MEVC|, representing the strength of ME couplings with applied H, shows a symmetrical mirror behavior respect to the *y* axis. For NZTFO/PZT/NZTFO tri-layer laminate, it increases rapidly with applied field to its maximum of 415 mV/cm Oe at optimum *H*=22Oe, and then levels off at its saturation of 38 mV/cm Oe. By contrast, for the bi-layered case the data in |MEVC| *vs H* profile shows its maximum of 215 mV/cm Oe at *H*=12Oe and then levels off at its saturation of 13 mV/cm Oe. Meanwhile, the strength of strain-mediated ME couplings is expected to be strong at EMR conditions, and it is established that the strongest ME interaction in ferromagnetic/ferroelectric laminate is achieved under EMR. Figure 7(b) illustrates MEVC *vs f* profile with frequency sweeping in the range of 54kHz-65kHz under optimum bias and the achievable maximum MEVC of 383 V/cm Oe is obtained at EMR frequency of 59.01kHz. For the NZTFO/PZT bi-layer case, MEVC with frequency sweeping in the range of 48 kHz-60kHz under optimum bias, and the achievable maximum MEVC reaches 225 V/cm Oe at EMR frequency of 54.19kHz. An enhancement of approximately 70% in MEVC was found in tri-layer ME composite relative to that in bi-layer ME composite, anticipating a higher eventual power conversion efficiency in this case.

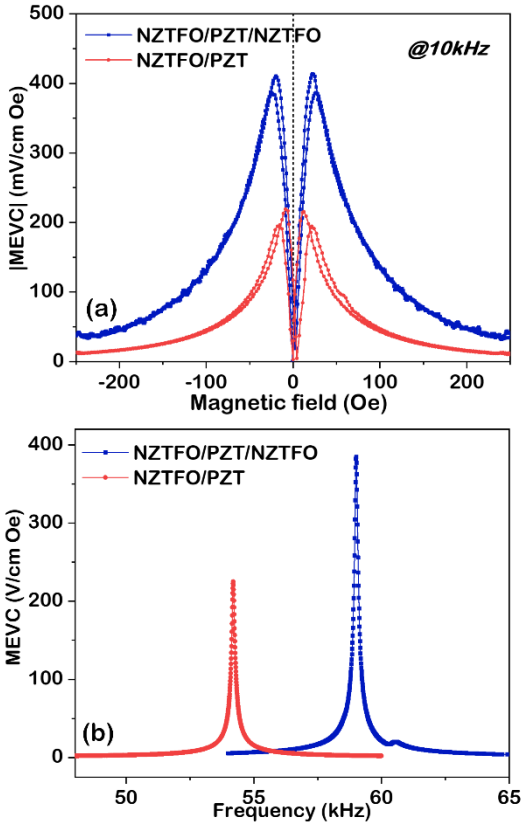


Fig.7(a) Off-resonance ME hysteretic responses at the frequency of 10kHz for NZTFO/PZT/NZTFO tri-layers and NZTFO/PZT bi-layers. (b) Resonance ME responses with frequency sweeping in the range of 54kHz-65kHz for NZTFO/PZT/NZTFO tri-layers and 48 kHz-60kHz for NZTFO/PZT bi-layers.

Generally, power conversion efficiency (PE) was employed to evaluate the capability of energy transfer in the dynamic magneto-mechanical-electric process for ME gyrators, thereby PE plays an irreplaceable role for the device design and deployable applications. Nevertheless, PE always reaches its maximum when the well-matched resistance load equals to the capacitive reactance at EMR driving. For PE characterizations, the input power of solenoid remains constant value of 1μW with the settings of function generator consistent in that for magneto-mechanical characterizations. Figure 8 shows the experimental results of induced voltage and PE variations for tri-layers and bi-layer samples as a function of load resistance *R*, respectively. As *R* is increased from 1Ω to 3.5kΩ, PE exhibits a precipitously rise to its maximum of ~80.3% and then shows a modest decrease with further increase in *R*. Meanwhile, the induced voltage exhibits an increasing tendency and then stabilizes at *R*=25kΩ with its saturation of 42.5mV. By contrast, similar measurements were implemented for bi-layer symmetrical ME composite. As a result, Fig. 8(b) shows the induced voltage and corresponding PE for NZTFO/PZT bi-layer composite, the induced voltage stabilizes at *R*=20kΩ with its saturation of 22.6mV and PE reaches its maximum of ~29.3% at 2.2kΩ and then levels off at 6.5% for *R*>20 kΩ. This means that more than 70% of energies were dissipated in the magneto-mechanical-electric conversion process for the bi-layer case, which is mainly attributed to halved actuating sources as well as more dissipated spatial energy field into the air. Similar results were reported on Terfenol-D/PZT laminate constituted ME-coil gyrators with the maximum PE of ~34.7% under *R*=1kΩ,[40] and PE measured in EMR frequency of 53.8kHz showed a maximum of ~43% under *R*=700Ω for PZT/NZFO sample.[41] Therefore, we infer from the results and

discussions that the main energy dissipation is related to the mechanical loss between layers, leading to weakened magneto-mechanical couplings for efficient energy transfer.

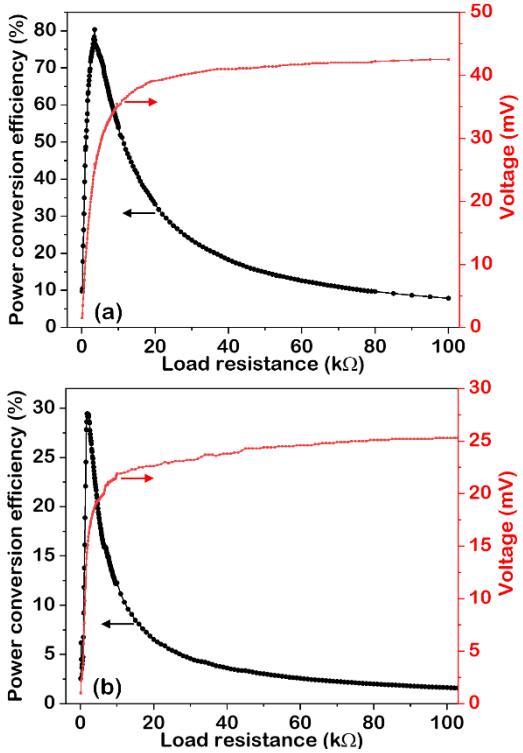


Fig.8(a) Power conversion efficiency and output voltage as a function of load resistance for the NZTFO/PZT/NZTFO tri-layer ME gyrator. (b) Power conversion efficiency and output voltage as a function of load resistance for the NZTFO/PZT bi-layer ME gyrator.

## 4. Conclusions

In summary, a non-contact optical measurement methodology was employed to disentangle the dynamic magneto-mechanical-electric conversion process quantitatively in ME-coil gyrators. The trapped efficient magnetic field induced vibrating velocity in ME samples was captured layer by layer through the focused laser beam, and then the converted kinetic energies can be calculated to evaluate the dissipated energies in this process quantitatively. In addition, measurements of low-frequency/resonance ME couplings and eventual PE were implemented for bi-layer and tri-layer ME gyrators for comparative studies. Experimental results show that approximately 29% and 43% strain-mediated energies were dissipated in tri-layer and bi-layer ME gyrators, respectively, and the mechanical loss between layers is still the main source of energy dissipations to restrict further improvement of conversion efficiencies. Meanwhile, an eventual maximum PE of 80.3% was obtained in tri-layer ME gyrator while the one of 29.3% for bi-layer case to support our inference. These findings provide an enlightening guidance and experimental evidence with enhanced flexibility for the ME gyrator design and fabrication.

## Acknowledgements

This research was financially supported by National Natural Science Foundation of China (NSFC) (Grant Nos. 61973279, 62004177, 62073299), Program for Innovative Research Group (in Science and Technology) in University of Henan Province（No.20IRTSTHN017). The study at Russia was supported by the Russian Foundation for Basic Research (Grant No. 18-52-00021). The

research at Oakland University was supported by a grant from the National Science Foundation (Grant No. DMR-1808892).

[1] B. D. H Tellegen, The gyrator, A new electric network element, Philips Res, 3 (1948) 81-101.

[2] I. Tatai and I. Zaharie, The energy transfer between the ports of an implemented gyrator using LM13700 operational transconductance amplifier, Review of Scientific Instruments, 83(11) (2012) 114702.

[3] S. Bosco, F. Haupt and D. P. DiVincenzo, Self-impedance-matched hall-effect gyrators and circulators, Physical Review Applied, 7(2) (2017) 024030.

[4] S. Singer, Gyrators application in power processing circuits, IEEE Transactions on Industrial Electronics IE-34, (3) (1987) 313-318.

[5] A. Cervera, M. Evzelman, M. M. Peretz and S. Ben-Yaakov, A high-efficiency resonant switched capacitor converter with continuous conversion ratio, IEEE Transactions on Power Electronics, 30(3) (2015) 1373-1382.

[6] A. Nagulu, N. Reiskarimian and H. Krishnaswamy, Non-reciprocal electronics based on temporal modulation, Nature Electronics, 3 (2020) 241–250.

[7] A. V. Carazo J. Ryu, K. Uchino and H. E. Kim, Magnetoelectric properties in piezoelectric and magnetostrictive laminate composites, Japanese Journal of Applied Physics, 40(8) (2001) 4948-4951.

[8] N. Pereira, A. C. Lima,S. Lanceros-Mendez, and P. Martins, Magnetoelectrics: Three Centuries of Research Heading towards the 4.0 Industrial Revolution, Materials (Basel), 13 (2020) 4033.

[9] D. K. Pradhan, S. Kumari and P. D. Rack,, Magnetoelectric Composites: Applications, Coupling Mechanisms, and Future Directions, Nanomaterials (Basel), 10 (2020) 2072.

[10] J. Zhai, J. Gao, C. De Vreugd, J. Li, D. Viehland, A. V. Filippov, M. I. Bichurin, D. V. Drozdov, G. A. Semenov and S. X. Dong, Magnetoelectric gyrator, European Physical Journal B, 71(3) (2009) 383-385.

[11] N. A. Spaldin and R. Ramesh, Advances in magnetoelectric multiferroics, Nature Materials, 18(3) (2019) 203-212.

[12] C. M. Leung, X. Zhuang , D. A. Friedrichs , J. F. Li, R. W. Erickson, V. Laletin, M. Popov, G. Srinivasan, and D. Viehland, Highly efficient solid state magnetoelectric gyrators, Applied Physics Letters, 111(12) (2017) 122904.

[13] J. Y. Zhai, J. F. Li, S. X. Dong, D. Viehland and M. I. Bichurin, A quasi(unidirectional) Tellegen gyrator, Journal of Applied Physics, 100(12) (2006) 124509.

[14] X. Z. Dai, Y. M. Wen, P. Li, J. Yang and M. Li, Energy harvesting from mechanical vibrations using multiple magnetostrictive/piezoelectric composite transducers, Sensors and Actuators A: Physical, 166(1) (2011) 94-101.

[15] J. Yang, Y. M. Wen, P. Li, X. H. Yue, Q. M. Yu and X. L. Bai, A two-dimensional broadband vibration energy harvester using magnetoelectric transducer, Applied Physics Letters, 103(24) (2013) 243903.

[16] J. J. Zhang J. Han, Y. W. Gao, A nonlinear magneto-mechanical-thermal-electric coupling model of Terfenol-D/PZT/Terfenol-D and Ni/PZT/Ni laminates, Journal of Magnetism and Magnetic Materials, 466(NOV.) (2018) 200-211.

[17] C. M. Leung, J. F. Li, D. Viehland and X. Zhuang, A review on applications of magnetoelectric composites: from heterostructural uncooled magnetic sensors, energy harvesters to highly efficient power converters, Journal of Physics D: Applied Physics, 51 (2018) 263002.

[18] C. Z. Dong C. Tu, Z. Q. Chu, H. H. Chen, X. F. Liang and N. X. Sun, A passive isolator realized by magnetoelectric laminate composites, Applied Physics Letters, 113(26) (2018) 262904.

[19] V. Loyau, A. Aubert, M. LoBue, and F. Mazaleyrat, Analytical modeling of demagnetizing effect in magnetoelectric ferrite/PZT/ferrite trilayers taking into account a mechanical coupling, Journal of Magnetism and Magnetic Materials, 426(mar.) (2017) 530-539.

[20] C. M. Leung, G. Sreenivasulu, X. Zhuang, X. Tang, M. Gao, J. R. Xu, J. F. Li, J. T. Zhang, G. Srinivasan and D. Viehland, A highly efficient self-biased nickel-zinc ferrite/Metglas/PZT magnetoelectric gyrator, Physica Status

Solidi-Rapid Research Letters, 12(5) (2018) 1800043.

[21] C. M. Leung, X. Zhuang, J. R. Xu, M. Gao, X. Tang, J. F. Li, P. Zhou, G. Srinivasan and D. Viehland, A dual-output magnetoelectric gyrator, Journal of Physics D: Applied Physics, 52(6) (2019) 065003.

[22] C. M. Leung, X. Zhuang, J. R. Xu, J. F. Li, G. Srinivasan and D. Viehland, Importance of composite parameters in enhanced power conversion efficiency of Terfenol-D/PZT magnetoelectric gyrators, Applied Physics Letters, 110(11) (2017) 112904.

[23] X. Zhuang, C. M. Leung, J. F. Li, G. Srinivasan and D. Viehland, Power conversion efficiency and equivalent input loss factor in magnetoelectric gyrators, IEEE Transactions on Industrial Electronics, 66(4) (2018) 2499-2505.

[24] C. M. Leung, G. Sreenivasulu, X. Zhuang, M. Gao, X. Tang, J. R. Xu, J. F. Li, G.Srinivasan, and D. Viehland, Stability enhancement of yttrium substituted nickel zinc ferrite/PZT magnetoelectric gyrators under high power conditions, Applied Physics Letters, 112(24) (2018) 242901.

[25] Tulshidas C. Darvadea, Pravin S. Kadhanea, Bharat G. Baraskara, Ajit R. Jamesb , V.R. Reddyc , Rahul C. Kambalea, Structural and multiferroic properties of trilayer green magnetoelectric $Co_{0.8}Ni_{0.2}Fe_2O_4/K_{0.25}Na_{0.75}NbO_3/Co_{0.8}Ni_{0.2}Fe_2O_4$ composite structure, Journal of Magnetism and Magnetic Materials, 505 (2020) 166733.

[26] R. Stampfli, G. Youssef Multiphysics computational analysis of multiferroic composite ring structures, International Journal of Mechanical ences, 177 (2020) 105573.

[27] C. M. Leung, X. Zhuang, M. Gao, X. Tang, J. Xu, J. Li, J. Zhang, G. Srinivasan and D. Viehland, Enhanced stability of magnetoelectric gyrators under high power conditions, Applied Physics Letters, 111(18) (2017) 182901.

[28] J. T. Zhang, W. W. Zhu, D. A. Filippov, W. He, D. Y. Chen, K. Li, S. T. Geng, Q. F. Zhang, L. Y. Jiang, L. Z. Cao, R. Timilsina and G. Srinivasan, Highly efficient power conversion in magnetoelectric gyrators with high quality factor, Review of Scientific Instruments, 90(01) (2019) 015004.

[29] X. Zhuang, M. Gao, X. Tang, C. M. Leung, J. R. Xu, G. Srinivasan, J. F. Li, H. S. Luo and D. Viehland, A piezoelectric Mn-doped PMN-PT/Metglas magnetoelectric gyrator: enhanced power efficiency at reduced size, IEEE Sensors Journal, 20(2) (2020) 752-759.

[30] M. Pourhosseiniasl, X. Y. Gao, S. Kamalisiahroudi, Z. H. Yu, Z. Q. Chu, J. K. Yang, H. Y. Lee and S. X. Dong, Versatile power and energy conversion of magnetoelectric composite materials with high efficiency via electromechanical resonance, Nano Energy, 70 (2020) 104506.

[31] X. Zhuang, C. M. Leung, J. Li, and D. Viehland, Power conversion process in magnetoelectric gyrators, Applied Physics Letters, 111(10) (2017) 103902.

[32] X. Zhuang, C. M. Leung, J. F. Li and D. Viehland, Estimation of the Intrinsic power efficiency in magnetoelectric laminates using temperature measurements, Sensors, 20(11) (2020) 3332.

[33] S. K. Mandal, G. Sreenivasulu, V. M. Petrov, and G. Srinivasan, Flexural deformation in a compositionally stepped ferrite and magnetoelectric effects in a composite with piezoelectrics, Applied Physics Letters, 96 (2010) 192502.

[34] A. Srinivas, Dong-Wan Kim, Kug Sun Hong, and S. V. Suryanarayana, Observation of ferroelectromagnetic nature in rare-earth-substituted bismuth iron titanate, Applied Physics Letters, 83 (2003) 2217.

[35] J. T. Zhang, D. Y. Chen, K. Li, D. A. Filippov, B. F. Ge, Q. F. Zhang, X. X. Hang, L. Z. Cao, and G. Srinivasan, Self-biased magnetoelectric gyrators in composite of samarium substituted nickel zinc ferrites and piezoelectric ceramics, AIP Advances, 9 (2019) 035137.

[36] J. T. Zhang, K. Li, D. Y. Chen, D. A. Filippov, Q. F. Zhang, S. Y. Li, X. Peng, J. Wu, R. Timilsina, L. Z. Cao, and G. Srinivasan, Field-orientation-dependent dynamic strain Induced anisotropic magnetoelectric responses in bi-layered Ferrite/Piezoelectric composites, Journal of Electronic Materials, 49 (2019) 1120-1130.

[37] J. G. Wan, Z. Y. Li, Y. Wang, M. Zeng, G. H. Wang, and J.-M. Liu, Strong flexural resonant magnetoelectric effect in Terfenol-D/epoxy-Pb(Zr,Ti)O3 bilayer, Applied Physics Letters, 86 (2005).

[38] L. Chen, P. Li , Y. M. Wen, and Y. Zhu, Resonance magnetoelectric couplings of piezoelectric ceramic and ferromagnetic constant-elasticity alloy composites with different layer structures, Journal of Alloys and Compounds, 555 (2013) 156-160.

[39] H. Greve, E. Woltermann, H. Quenzer, B. Wagner and E. Quandt, Giant magnetoelectric coefficients in $(Fe_{90}Co_{10})_{78}Si_{12}B_{10}$-AlN thin film composites, Applied Physics Letters, 96 (2010) 182501.

[40] C. M. Leung, X. Zhuang, J. R. Xu, G. Srinivasan, J. F. Li, and D. Viehland, Power conversion efficiency and resistance tunability in coil-magnetoelectric gyrators, Applied Physics Letters, 109(20) (2016) 202907.

[41] J. T. Zhang, W. W. Zhu, D. Y. Chen, H. W. Qu, P. Zhou, M. Popov, L. Y. Jiang, L. Z. Cao and G. Srinivasan, Magnetoelectric effects and power conversion efficiencies in gyrators with compositionally-graded ferrites and piezoelectrics, Journal of Magnetism and Magnetic Materials, 473 (2019) 131-135.